Energy dispersion of the electrosubbands in parabolic confining quantum wires: interplay of Rashba, Dresselhaus, lateral spin–orbit interaction and the Zeeman effect

2009 J. Phys.: Condens. Matter 21 335501

(http://iopscience.iop.org/0953-8984/21/33/335501)

IOP Publishing Journal of Physics: Condensed Matter

J. Phys.: Condens. Matter **21** (2009) 335501 (9pp) doi:10.1088/0953-8984/21/33/335501

Energy dispersion of the electrosubbands in parabolic confining quantum wires: interplay of Rashba, Dresselhaus, lateral spin–orbit interaction and the Zeeman effect

Tong-Yi Zhang, Wei Zhao and Xue-Ming Liu

State Key Laboratory of Transient Optics and Photonics, Xi'an Institute of Optics and Precision Mechanics, Chinese Academy of Sciences, No. 17 Xinxi Road, Xi'an 710119, People's Republic of China

Received 21 November 2008, in final form 8 July 2009
Published 27 July 2009
Online at stacks.iop.org/JPhysCM/21/335501

Abstract

We have made a thorough theoretical investigation of the interplay of spin–orbit interactions (SOIs) resulting from Rashba, Dresselhaus and the lateral parabolic confining potential on the energy dispersion relation of the spin subbands in a parabolic quantum wire. The influence of an applied external magnetic field is also discussed. We show the interplay of different types of SOI, as well as the Zeeman effect, leads to rather complex and intriguing electrosubbands for different spin branches. The effect of different coupling strengths and different magnetic field strengths is also investigated.

(Some figures in this article are in colour only in the electronic version)

1. Introduction

In recent years, spin-dependent phenomena in semiconductors have been intensively investigated because of their potential for future spin electronic (or spintronics) devices [1–9]. In spintronic devices, the spin degree of freedom of electrons, together with their charge, is used for realizing new device concepts. These devices promise increased speed and lower power consumption, and may offer new functionalities having no counterpart in conventional electronic devices. In order to manipulate the electron spin by means of an electric field rather than by a magnetic field, many of these proposed device structures rely on the spin–orbit interaction (SOI). Two basic mechanisms of the SOI are Rashba coupling [10] and Dresselhaus coupling [11]. The former is caused by structural inversion asymmetry due to the triangular potential well confining carriers in the plane of the electron gas, while the latter is caused by bulk inversion asymmetry in noncentrosymmetric materials. The spin–orbit coupling parameter can be extracted from the characteristic beating pattern in the magnetoresistance of a two-dimensional electron gas [12] and can be controlled and manipulated by conventionally adjusting a gate voltage [13]. This property is the basis of the ballistic spin transistor proposed by Datta and Das [14] and the nonballistic spin transistor by Schliemann *et al* [15].

In the past two decades, much work has been done on the spin–orbit interaction of two-dimensional electron gases (2DEG) [16]. It has been shown that a restriction to a one-dimensional channel is more appropriate to further improve the performance of a spin transistor. Furthermore, a number of novel concepts of spintronic devices relying on one-dimensional carrier transport have been suggested [17–23]. Hence, the spin-dependent transport in one-dimensional quantum wires with SOI have attracted a great deal of attention. For example, the influence of Rashba SOI on the transport in one-dimensional systems at zero magnetic field was theoretically investigated by Moroz and Barnes [24, 25] and Mireles and Kirczenow [26]. The transport properties in the presence of a magnetic field perpendicular to the quantum well plane have also been investigated both theoretically [27–30] and experimentally [31–33]. Knobbe and Schäpers [28] have demonstrated that the quantization due to the carrier

confinement in a one-dimensional system with Rashba SOI, compared to the case of a 2DEG, results in a modification of the beating pattern of the magnetoresistance. Recently, Lehnen *et al* [34] have shown the spin–orbit scattering length is enhanced in narrow wires. Also the optical absorption in quantum wires with SOI have been investigated [35, 36].

Physical properties of condensed matter systems are often determined by the energy spectrum of charge carriers. Much work has been devoted to investigate the spin–orbit effects on the energy dispersion of 2DEG. Das *et al* [37] have applied the tilted magnetic field technique to deduce the zero-field splittings of 2D InGaAs/InAlAs heterostructures. The interplay between the Zeeman, Rashba and Dresselhaus interactions in quantum wells has been discussed in relation to the violation of the Larmor theorem due to the SOIs [38] and with the spin splitting of the Landau levels, charge- and spin-density excitations [39] using an approximate analytical solution of the quantum well SOI Hamiltonian. The interplay between Zeeman and SOI has also been discussed in [40] using the unitarily transformed Hamiltonian technique. This interplay is very important for some specific devices, such as for the nonballistic spin transistor [15]. The situation is more intriguing for quantum wires. In the presence of an external magnetic field, the interplay of magnetic field, the SOI and the transverse confinement of quantum wires leads to complicated and intriguing energy dispersion and magnetotransport properties. Magnetosubbands of semiconductor quantum wires with Rashba but without Dresselhaus SOI under a magnetic field have been calculated by Knobbe and Schäpers [28]. Pramanik *et al* [41] have calculated magnetosubbands of semiconductor quantum wires in the presence of both Rashba and Dresselhaus SOI, where the transverse confinement is assumed an infinite high rectangular well potential (hard-wall boundary conditions). The effect of an in-plane magnetic field on the electron transport in quasi-one-dimensional systems has also been calculated [42–44]. Bandyopadhyay *et al* [45] have derived the magnetoelectric subbands and eigenstates in a quantum wire with Rashba and Dresselhaus SOI for three different orthogonal orientations of the external magnetic field, but their derivations are limited to only the lowest magnetoelectric subband. Tserkovnyak and Halperin [46] have investigated theoretically the magnetoconductance of cylindrical quasi-one-dimensional nanowires carrying several quantum channels confined near the surface. More recently, Sánchez *et al* [47] have analyzed theoretically the transport properties of a ballistic quantum wire with a spatially inhomogeneous Rashba interaction in the presence of an external magnetic field giving rise to Zeeman spin splitting.

In the works mentioned above, some spin–orbit interactions have been neglected. But for strongly confined quantum wires, spin–orbit interactions due to different mechanisms may be present simultaneously. To the best of our knowledge, however, the effect due to the interplay among them has not been analyzed thoroughly. In this paper, we investigate theoretically the interplay of Rashba and Dresselhaus SOI, as well as the SOI due to a parabolic lateral confining potential and the Zeeman effect in a semiconductor quantum wire. We show that the interplay of SOI due to different mechanisms and the Zeeman effect leads to richer structures. The difference in the dispersion due to different spin–orbit interactions and the their interplay would lead to different transport and optical properties, which may be used to identify the existence of specific spin–orbit coupling mechanisms. This paper is organized as follows. In section 2, we present our model describing Rashba and Dresselhaus SOI, and the SOI due to lateral confinement in a parabolic quantum wire. In section 3, numerical results of the energy dispersion relation for electrosubbands are presented and discussed for different spin–orbit coupling parameters and magnetic field strength. We first discuss the interplay of the three different types of SOI in the absence of an external magnetic field in section 3.1. Then in section 3.2, a magnetic field is applied to the quantum wire and the influence of the Zeeman effect is included. Conclusions are presented in section 4.

2. Theoretical model

We consider a quantum wire defined by split gates on a two-dimensional electron gas confined in a semiconductor quantum well. We take the growth direction of the quantum well to be along the z direction, the transverse lateral confinement is along the x direction and the quantum wire is along the y direction. We assume the quantum wire is relatively narrow and the transverse confinement is well approximated as a parabolic potential expressed by

$$V(x) = \tfrac{1}{2}m^*\omega_0^2 x^2, \tag{1}$$

with the oscillator frequency given by ω_0. We assume an external magnetic field oriented along the z direction is applied to the quantum wire, $\mathbf{B} = (0, 0, B)$, and take the vector potential in the Landau gauge, $\mathbf{A} = Bx\mathbf{e}_y = (0, Bx, 0)$. We assume that the quantum well is sufficiently thin and only the lowest subband in the z direction needs to be considered. Thus, the single-particle Hamiltonian of the quantum wire is then given by $H = H_0 + H_{\rm so}$, where

$$H_0 = \frac{1}{2m^*}(\mathbf{p} + e\mathbf{A})^2 + V(x) + \frac{1}{2}g^*\mu_{\rm B}\boldsymbol{\sigma}\cdot\mathbf{B}, \tag{2}$$

is the part without SOI and $H_{\rm so}$ represents the SOI Hamiltonian, respectively. The first term in H_0 is the kinetic contribution with m^* the effective electron mass and $\mathbf{p}$ the electron momentum vector, while the last term in H_0 is the Zeeman energy splitting with g^* the effective Landé gyromagnetic factor, $\mu_{\rm B} = \frac{e\hbar}{2m_0c}$ the Bohr magneton and $\boldsymbol{\sigma}$ the well-known Pauli spin matrix vector with $\sigma_x = \left(\begin{smallmatrix}0 & 1\\ 1 & 0\end{smallmatrix}\right)$, $\sigma_y = \left(\begin{smallmatrix}0 & -\mathrm{i}\\ \mathrm{i} & 0\end{smallmatrix}\right)$, $\sigma_z = \left(\begin{smallmatrix}1 & 0\\ 0 & -1\end{smallmatrix}\right)$. Substituting the vector potential and magnetic field vector, H_0 can be explicitly written as

$$H_0 = \frac{1}{2m^*}[p_x^2 + (p_y + eBx)^2] + V(x) + \frac{1}{2}g^*\mu_{\rm B}\sigma_z B. \tag{3}$$

The general form of the SOI Hamiltonian is derived from the quadratic in υ/c expansion of the Dirac equation [24, 48]

$$H_{\rm so} = \frac{\hbar}{(2m^*c)^2}\nabla V(\mathbf{r})\cdot\boldsymbol{\sigma}\times\mathbf{p} = -\frac{\hbar}{(2m^*c)^2}\mathbf{E}(\mathbf{r})\cdot\boldsymbol{\sigma}\times\mathbf{p}. \tag{4}$$

This universal form does not restrict us to any particular model of the potential $V(\mathbf{r})$. Although this SOI has an essentially relativistic nature, it nevertheless can give rise to an observable modification of semiconductor band structure. For the quantum wire considered here, Rashba SOI, Dresselhaus SOI and the SOI due to the lateral parabolic confining potential can arise.

The Rashba SOI arises from the asymmetry of the quantum well induced by an uniform interface induced field or by an external applied gate voltage along the z direction. The Rashba SOI Hamiltonian is given by

$$H_{\mathrm{R}} = \frac{\alpha_{\mathrm{R}}}{\hbar}\mathbf{e}_z[\boldsymbol{\sigma}\times(\mathbf{p}+e\mathbf{A})] = \frac{\alpha_{\mathrm{R}}}{\hbar}[\sigma_x(p_y+eBx)-\sigma_y p_x], \quad (5)$$

where α_{R} is the Rashba spin–orbit coupling parameter, which can be varied by the gate electric field E_z.

The Dresselhaus SOI Hamiltonian is given by

$$H_{\mathrm{D}} = \frac{\beta_{\mathrm{D}}}{\hbar}\boldsymbol{\sigma}\cdot\boldsymbol{\kappa}, \quad (6)$$

where β_{D} is the Dresselhaus spin–orbit coupling parameter, which depends on the effective width and thickness of the quantum wire and can be varied with a split gate potential that controls the oscillator frequency (thus the effective width). As mentioned above, we assume that the thickness of the quantum wire is sufficiently thin such that $\langle p_z^2\rangle \gg \langle p_y^2\rangle, \langle p_x^2\rangle$. Then, substituting the vector potential, the components of the vector $\boldsymbol{\kappa} = (\kappa_x, \kappa_y, \kappa_z)$ can be written in a simplified form [41]:

$$\begin{aligned}\kappa_x &= \tfrac{1}{2}\{(p_x+eA_x)[(p_y+eA_y)^2-(p_z+eA_z)^2]\\ &\quad+[(p_y+eA_y)^2-(p_z+eA_z)^2]\\ &\quad\times(p_x+eA_x)\}\approx -p_x p_z^2, \quad (7)\\ \kappa_y &= \tfrac{1}{2}\{(p_y+eA_y)[(p_z+eA_z)^2-(p_x+eA_x)^2]\\ &\quad+[(p_z+eA_z)^2-(p_x+eA_x)^2]\\ &\quad\times(p_y+eA_y)\}\approx (p_y+eBx)p_z^2, \quad (8)\\ \kappa_z &= \tfrac{1}{2}\{(p_z+eA_z)[(p_x+eA_x)^2-(p_y+eA_y)^2]\\ &\quad+[(p_x+eA_x)^2-(p_y+eA_y)^2]\\ &\quad\times(p_z+eA_z)\}\approx p_z[p_x^2-(p_y+eBx)^2]. \quad (9)\end{aligned}$$

Therefore, the Dresselhaus spin–orbit Hamiltonian can be approximated as

$$H_{\mathrm{D}} \approx \frac{\beta_{\mathrm{D}}}{\hbar}p_z^2[\sigma_y(p_y+eBx)-\sigma_x p_x], \quad (10)$$

by neglecting the $\sigma_z\kappa_z$ term due to $\langle p_z\rangle = 0$. Thus, the Dresselhaus spin–orbit coupling parameters are dependent on the subband index in the z direction. Since we assume that the quantum well is sufficient thin and consider only the lowest subband in the z direction, thus we take the effective Dresselhaus spin–orbit coupling parameter as a constant $\beta_{\mathrm{D}}' = \beta_{\mathrm{D}}\langle p_z^2\rangle$. Hereafter, we still use β_{D} instead of β_{D}' in the remaining parts in our paper, i.e.

$$H_{\mathrm{D}} = \frac{\beta_{\mathrm{D}}}{\hbar}[\sigma_y(p_y+eBx)-\sigma_x p_x]. \quad (11)$$

From the general form of the SOI Hamiltonian (4), the Hamiltonian of the SOI coming from the transverse confining potential is [27]

$$H_{\mathrm{so}}^{\mathrm{T}} = \frac{\gamma}{\hbar}\frac{x}{l_0}\mathbf{e}_x[\boldsymbol{\sigma}\times(\mathbf{p}+e\mathbf{A})] = \frac{\gamma}{\hbar}\frac{x}{l_0}\sigma_z(p_y+eBx). \quad (12)$$

Here, γ is the spin–orbit coupling parameter and we neglect the term $\sigma_y p_z$ due to $\langle p_z\rangle = 0$. We have also introduced a length scale characterizing the strength of the lateral confining potential $l_0 = \sqrt{\hbar/m^*\omega_0}$. In addition to l_0, for the quantum wire considered, another four length scales can be introduced to characterize the relative strengths of the magnetic field, the Rashba SOI, the Dresselhaus SOI and the SOI due to the transverse potential, respectively:

$$\begin{aligned} l_B &= \sqrt{\hbar/eB} = \sqrt{\hbar/m^*\omega_{\mathrm{c}}}, \qquad l_{\mathrm{R}} = \hbar^2/2m^*\alpha_{\mathrm{R}},\\ l_{\mathrm{D}} &= \hbar^2/2m^*\beta_{\mathrm{D}}, \qquad l_{\mathrm{T}} = \hbar^2/2m^*\gamma, \end{aligned} \quad (13)$$

Correspondingly, there are five energy scales characterizing the relative strengths, respectively:

$$\begin{aligned} &\hbar\omega_0, \qquad \hbar\omega_{\mathrm{c}}, \qquad \Delta_{\mathrm{R}} = \frac{m^*\alpha_{\mathrm{R}}^2}{2\hbar^2},\\ &\Delta_{\mathrm{D}} = \frac{m^*\beta_{\mathrm{D}}^2}{2\hbar^2}, \qquad \Delta_{\mathrm{T}} = \frac{m^*\gamma^2}{2\hbar^2}. \end{aligned} \quad (14)$$

where $\omega_{\mathrm{c}} = eB/m^*$ is the cyclotron frequency.

Thus, the explicitly expressed total Hamiltonian is

$$\begin{aligned} H &= \frac{1}{2m^*}p_x^2 + \frac{1}{2m^*}(p_y+eBx)^2 + \frac{1}{2}m^*\omega_0^2x^2 + \frac{1}{2}g\mu_{\mathrm{B}}B\sigma_z\\ &\quad+\frac{\alpha_{\mathrm{R}}}{\hbar}[\sigma_x(p_y+eBx)-\sigma_y p_x]\\ &\quad+\frac{\beta_{\mathrm{D}}}{\hbar}[\sigma_y(p_y+eBx)-\sigma_x p_x]+\frac{\gamma}{\hbar}\frac{x}{l_0}\sigma_z(p_y+eBx). \end{aligned} \quad (15)$$

Due to the complex coupling between spin subbands in the total Hamiltonian (15), we suppose that no analytic solution of the Schrödinger equation can be obtained, apart from some trivial limits. Therefore, we must solve the Schrödinger equation numerically to achieve an insight about the interplay of the SOI arising from different mechanisms.

Since the total Hamiltonian H is translationally invariant along the wire, plane waves are taken along the y direction, with wave numbers k_y a good quantum number of the system. We take the ansatz

$$\Psi(x, y) = \phi(x)\exp(\mathrm{i}k_y y), \quad (16)$$

so that the Schrödinger equation becomes separable in x and y. By applying this ansatz, the Hamiltonian H_0 reduces to

$$H_0 = \left[-\frac{\hbar^2}{2m^*}\frac{\mathrm{d}^2}{\mathrm{d}x^2}+\frac{1}{2}m^*\omega^2(x-x_0)^2+\frac{\omega_0^2}{\omega^2}\frac{\hbar^2k_y^2}{2m^*}\right]+\frac{1}{2}g\mu_{\mathrm{B}}B\sigma_z, \quad (17)$$

and the spin–orbit Hamiltonian H_{so} reduces to

$$H_{so} = \alpha_R\left[\sigma_x\left(k_y + \frac{eB}{\hbar}x\right) + i\sigma_y\frac{d}{dx}\right] + \beta_D\left[\sigma_y\left(k_y + \frac{eB}{\hbar}x\right) + i\sigma_x\frac{d}{dx}\right] + \gamma\frac{x}{l_0}\sigma_z\left(k_y + \frac{eB}{\hbar}x\right). \quad (18)$$

Here, $\omega = (\omega_c^2+\omega_0^2)^{1/2}$ is the effective oscillator frequency and $x_0 = -(\omega_c/\omega)^2(\hbar k_y/eB) = -(\omega_c/\omega)^2 l_B^2 k_y$ is the guiding-center coordinate for the harmonic oscillator.

The set of eigenfunctions of H_0 obtained from the Schrödinger equation for the system without spin–orbit coupling $H_0\phi_{n\sigma}(x) = E_{n\sigma}^{(0)}\phi_{n\sigma}(x)$ is given by

$$\phi_{n\sigma}(x) = \frac{1}{\sqrt{\sqrt{\pi}l_\omega 2^n n!}}H_n\left(\frac{x-x_0}{l_\omega}\right) \times \exp\left(-\frac{1}{2}\left(\frac{x-x_0}{l_\omega}\right)^2\right)\chi_\sigma, \quad \text{with } n = 0, 1, 2, \ldots; \quad \sigma = \pm, \quad (19)$$

with $l_\omega = \sqrt{\hbar/m^*\omega}$ the characteristic length of the harmonic oscillator with the effective oscillator frequency, $H_n(x)$ are the Hermite polynomials of integer order n, while $\chi_+ = \binom{1}{0}$ and $\chi_- = \binom{0}{1}$ are the spinors for up- and down-spin projected in the z direction, respectively. The corresponding energy eigenvalues are given by

$$E_{n\pm}^{(0)} = \hbar\omega\left(n + \frac{1}{2}\right) + \frac{\hbar^2}{2m^*}\frac{\omega_0^2}{\omega^2}k_y^2 \pm \frac{1}{2}g\mu_B B. \quad (20)$$

By expanding the transverse wavefunction $\phi(x)$ in the basis of the eigenfunctions $\phi_{n\sigma}(x)$ of H_0, $\phi(x) = \sum_{n\sigma} a_{n\sigma}\phi_{n\sigma}(x)$, we can obtain the following equations for the expanding coefficients:

$$(E_{n\sigma}^{(0)} - E)a_{n\sigma} + \sum_{m,\sigma'}(H_{so})_{nm}^{\sigma\sigma'}a_{m\sigma'} = 0. \quad (21)$$

The matrix elements $(H_R)_{nm}^{\sigma\sigma'} = \langle\phi_{n\sigma}|H_R|\phi_{m\sigma'}\rangle$ are given by

$$(H_R)_{nn}^{\pm\mp} = \alpha_R\left(1 - \frac{\omega_c^2}{\omega^2}\right)k_y, \quad (22)$$

$$(H_R)_{nm}^{\pm\mp} = \frac{\alpha_R}{l_\omega}\left\{\left(\frac{\omega_c}{\omega} \pm 1\right)\sqrt{\frac{n+1}{2}}\delta_{n,m-1} + \left(\frac{\omega_c}{\omega} \mp 1\right)\sqrt{\frac{n}{2}}\delta_{n,m+1}\right\}, \quad n \geqslant 1. \quad (23)$$

The matrix elements $(H_D)_{nm}^{\sigma\sigma'} = \langle\phi_{n\sigma}|H_D|\phi_{m\sigma'}\rangle$ are given by

$$(H_D)_{nn}^{\pm\mp} = \pm i\beta_D\left[1 - \left(\frac{\omega_c}{\omega}\right)^2\right]k_y, \quad (24)$$

$$(H_D)_{nm}^{\pm\mp} = (\pm i)\frac{\beta_D}{l_\omega}\left\{\left(\frac{\omega_c}{\omega} \pm 1\right)\sqrt{\frac{n}{2}}\delta_{n,m+1} + \left(\frac{\omega_c}{\omega} \mp 1\right)\sqrt{\frac{n+1}{2}}\delta_{n,m-1}\right\}, \quad n \geqslant 1. \quad (25)$$

The matrix elements $(H_{so}^T)_{nm}^{\sigma\sigma'} = \langle\phi_{n\sigma}|H_{so}^T|\phi_{m\sigma'}\rangle$ are given by

$$(H_{so}^T)_{nn}^{\pm\pm} = \pm\left(\frac{\gamma}{l_0}\right)\left(\frac{\omega_c}{\omega}\right)\left\{\left(n + \frac{1}{2}\right) - \left(\frac{\omega_c}{\omega}\right)l_B^2 k_y^2\left[1 - \left(\frac{\omega_c}{\omega}\right)^2\right]\right\} \quad (26)$$

$$(H_{so}^T)_{n,m\neq n}^{\pm\pm} = \pm\frac{\gamma}{l_0}k_y l_\omega\left[\sqrt{\frac{n}{2}}\delta_{n,m+1} + \sqrt{\frac{n+1}{2}}\delta_{n,m-1}\right] \pm \frac{1}{2}\frac{\gamma}{l_0}\left(\frac{\omega_c}{\omega}\right)\left[\sqrt{n(n-1)}\delta_{n,m+2} + \sqrt{(n+1)(n+2)}\delta_{n,m-2}\right]. \quad (27)$$

The matrix elements $(H_{R(D)})_{nn}^{\pm\mp}$ couple opposite spins within a given state n, whereas $(H_{R(D)})_{nm}^{\pm\mp}$ couple neighboring oscillator-level states with opposite spins due to the Rashba (Dresselhaus) SOI, respectively. The matrix elements $(H_{so}^T)_{nn}^{\pm\pm}$ lead to a level shift of oscillator-level states, whereas $(H_{so}^T)_{n,m\neq n}^{\pm\pm}$ couple neighboring and next-neighboring oscillator-level states with the same spins. From the matrix elements $(H_{so}^T)_{nn}^{\pm\pm}$, we can see that the spin-slitting due to the lateral spin–orbit coupling is n-dependent, which results in the separation between different spin orientations within a given state is larger for higher oscillator levels. By exact numerical diagonalization of equation (21), the energy dispersion relations and eigenfunctions of the magnetoelectric subband in the wire can be obtained.

3. Numerical results and discussions

The actual strengths of Rashba and Dresselhaus SOIs are discussed in many papers and it is believed that both of them can be tuned to be of the same order [15]. In addition, the strengths of Rashba and Dresselhaus SOIs in a quantum wire can be varied with external gate potentials [49]. Then, if the lateral confinement is sufficiently strong, the electric field induced by the spatial non-uniformity of the confinement potential may not be negligible in comparison with the Rashba and Dresselhaus fields. Thus, we vary all three SOI strengths over a wide range in this paper in order to elucidate the interplay of different SOIs. We calculate the energy dispersion relations of the subbands in the quantum wire by solving equation (21) through an exact diagonalization. In section 3.1. Then the interplay of the three different types of SOI in the absence of an external magnetic field is discussed. Then in section 3.2, we apply an external magnetic field to the quantum wire and discuss the influence of the magnetic field and Zeeman effect.

3.1. Without magnetic field

To identify the interplay of various SOIs due to different mechanisms in the absence of an external magnetic field, we present first in figure 1 the energy dispersion of a parabolic confining quantum wire with an individual mechanism. Figure 1 shows the energy dispersion in the presence of an individual SOI mechanism with weak ($\Delta_{so}/\hbar\omega_0 = 0.01$) (figures 1(a) and (b)), moderate ($\Delta_{so}/\hbar\omega_0 = 0.1$) (figures 1(c) and (d)) and strong ($\Delta_{so}/\hbar\omega_0 = 1$) (figures 1(e) and (f))

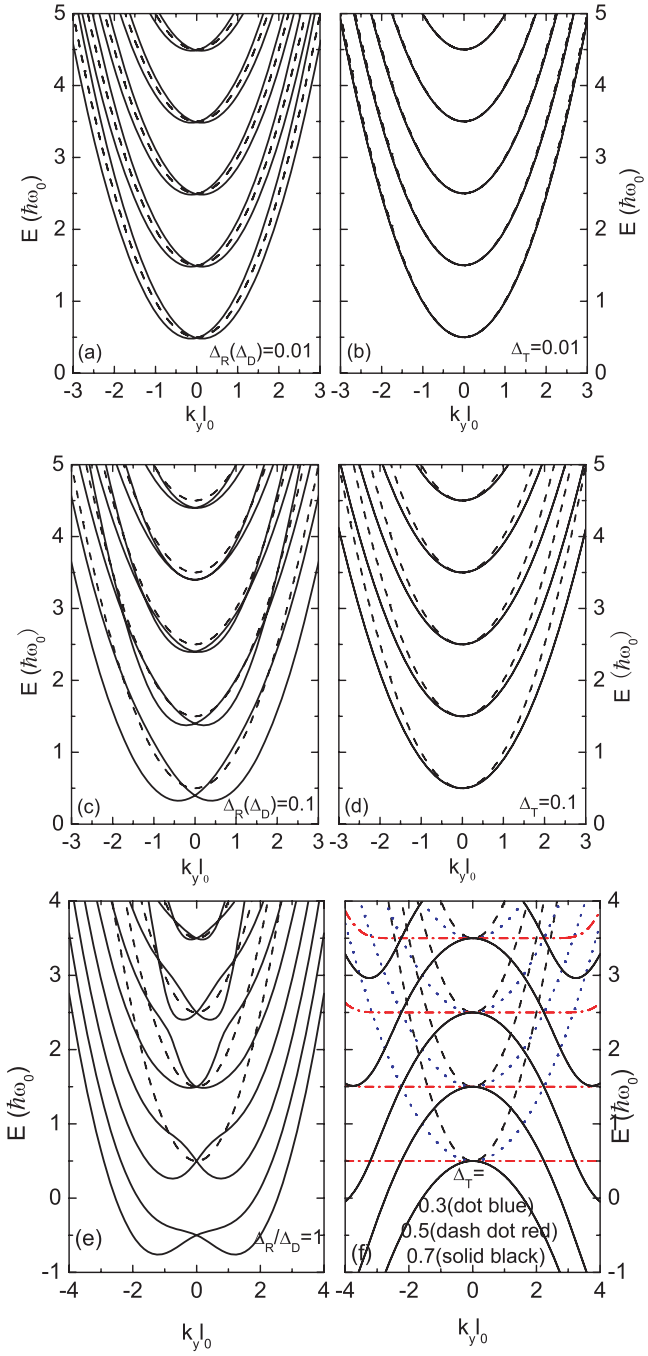

Figure 1. Energy dispersion of the spin-split subbands at $B = 0$ for weak $\Delta_{so} = 0.01$ ((a) and (b)), moderate $\Delta_{so} = 0.1$ ((c) and (d)), and strong $\Delta_{so} = 1$ ((e) and (f)) coupling. (a), (c) and (e) for Rashba or Dresselhaus spin–orbit coupling, respectively. (b), (d) and (f) for spin–orbit coupling due to parabolic transverse confining potential. (Δ_R, Δ_D and Δ_T are in units of $\hbar\omega_0$.)

coupling parameters, respectively. The energy dispersion in the absence of SOI is also presented as dashed lines for comparison. Since the energy dispersion caused by Rashba or Dresselhaus SOI are the same for the same characteristic spin–orbit energy (i.e. $\Delta_R = \Delta_D = \Delta_{so}$), we label one SOI parameter with the other in parentheses in figures 1(a), (c), and (e), respectively. The energy dispersion caused by the SOI due to the lateral confinement potential in different coupling strengths is shown in figures 1(b), (d), and (f), respectively. In all figures presented in this paper, the energy scales are in units of $\hbar\omega_0$.

For a weak Rashba (or Dresselhaus) SOI, the twofold-degenerate parabola for the two different spin orientations within each subband splits into two horizontal displaced parabolas with a degeneracy point at $k_y = 0$. The coupling between different subbands is negligible. A moderate Rashba SOI leads to weak anticrossings between different spin orientations within the same subband that occur at lower k_y values than the k_y values at which weak coupling occurs between different spin orientations and different neighboring subbands. For a strong Rashba (or Dresselhaus) SOI, the anticrossings for different spin orientation in neighboring subbands are pronounced and occur at k_y values, while the anticrossings for different spin orientation within each subband are weak and occur at higher k_y values. In addition, the SOI results in an uniformly downward energy shift of the subbands by Δ_{so} compared to the unperturbed system at the degeneracy points at $k_y = 0$ [18, 50]. Eto *et al* [21] have discussed the energy subbands in a hard-wall quantum wire and suggested that a semiconductor point contact can be used as a spin polarization filter. However, there are some differences in the energy dispersion of the subbands between their results and ours. In our case, the interplay of the parabolic confinement and the spin–orbit coupling gives rise to coupling between different spins within the same subband as terms (22) and (24), and thus leads to anticrossing within the same subband as shown in figure 1(c). These anticrossings are absent as the coupling terms would disappear for hard-wall confinement potential. Another different point is that the anticrossing due to spin–orbit interaction is negligible for very weak coupling (compared with the strength of the lateral confining potential $\hbar\omega_0$) as shown in figure 1(a). But this suppression is absent for a hard-wall confinement potential as there is no such energy scaling.

On the other hand, the SOI due to the lateral confinement does not change the twofold spin degeneracy of the energy dispersion for all quantum levels at all values of k_y, but they decrease the slope of the parabolic energy subbands for a weak and a moderate spin–orbit coupling parameter. Because the last term in (15) depends linearly on coordinate x in the absence of magnetic field, the matrix elements of this linear term are zero for both spin orientations within the same subband. Only in the presence of a magnetic field, which leads to an additional quadratically x-dependent term, do we have non-zero matrix elements for both spin orientations within the same subband, as shown in (26). From figure 1(f), we see that, when $\Delta_R = 0.5$, the subband bottoms become flat and the width of the flat bottom is narrower for higher subbands. When $\Delta_R < 0.5$, the dispersion remain parabolic but with a flattened slope, while for $\Delta_R > 0.5$, the dispersion becomes a parabola with negative slopes for small values of k_y and then changes into a parabola with positive slopes for large values of k_y. The inflection of the slopes changing from negative to positive becomes close to the zero point of k_y as the subband index n increases.

Having learned the effect of individual SOIs, we now turn to the interplay of the different types of SOIs on electronic

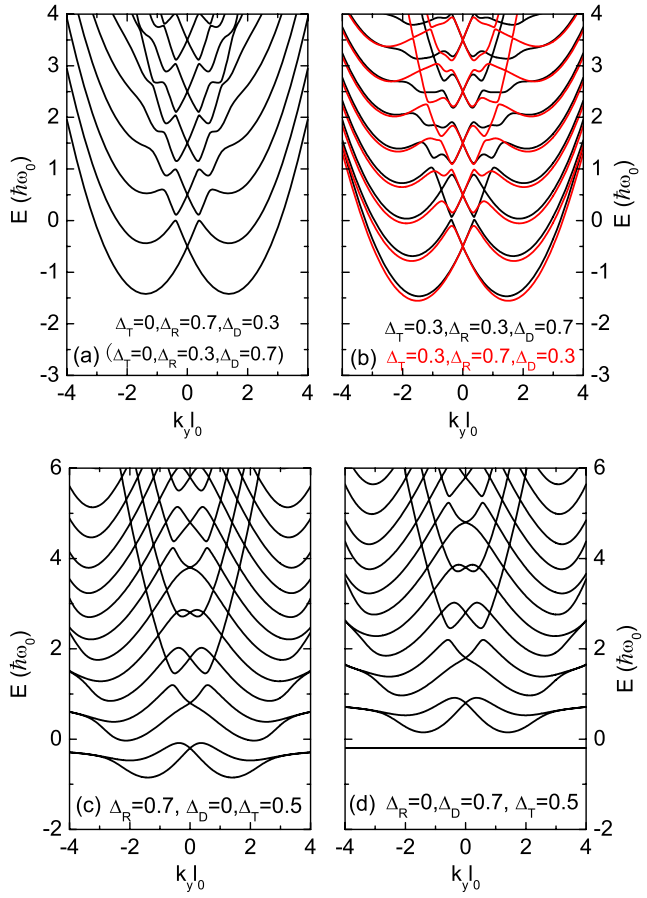

Figure 2. Energy dispersion of the spin-split subbands at $B = 0$ for cases where spin–orbit interactions due to different mechanisms present simultaneously and the coupling strength of Rashba and Dresselhaus spin–orbit interaction are different. (a) $\Delta_R = 0.7$ and $\Delta_D = 0.3$, or vice versa, for $\Delta_T = 0$. (b) $\Delta_R = 0.7$ and $\Delta_D = 0.3$ (black), or vice versa (red), for $\Delta_T = 0.3$. (c) $\Delta_R = 0.7$, $\Delta_D = 0$, and $\Delta_T = 0.5$. (d) $\Delta_R = 0$, $\Delta_D = 0.7$, and $\Delta_T = 0.5$. (Δ_R, Δ_D and Δ_T are in units of $\hbar\omega_0$.)

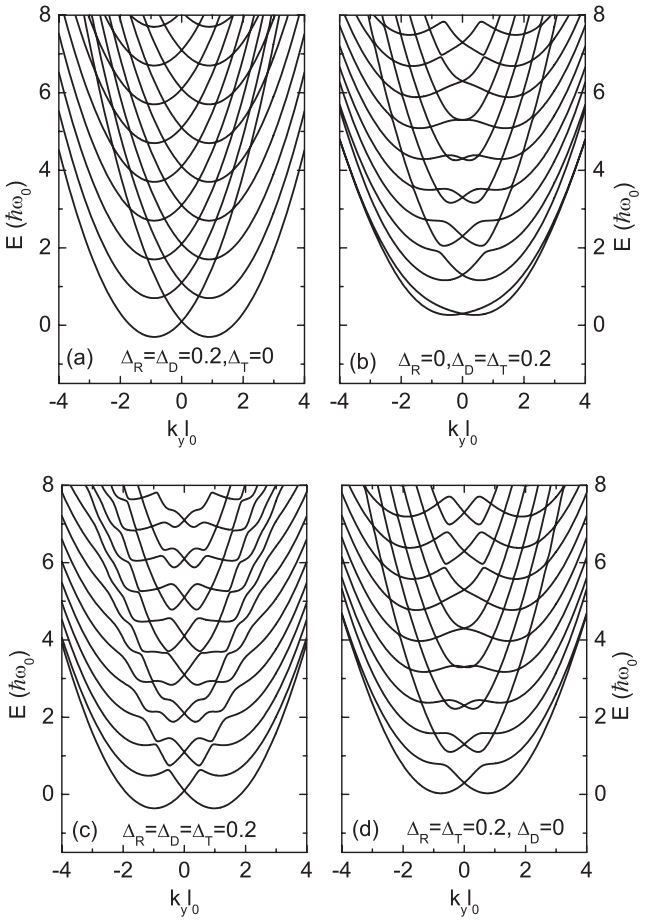

Figure 3. Energy dispersion of the spin-split subbands at $B = 0$ for cases where spin–orbit interactions due to different mechanisms present simultaneously and at least two of the coupling strengths are equal. (a) $\Delta_R = \Delta_D = 0.2$, $\Delta_T = 0$. (b) $\Delta_R = 0$, $\Delta_D = \Delta_T = 0.2$. (c) $\Delta_R = \Delta_D = \Delta_T = 0.2$. (d) $\Delta_R = \Delta_T = 0.2$, $\Delta_D = 0$. (Δ_R, Δ_D and Δ_T are in units of $\hbar\omega_0$.)

energy dispersion. In figure 2(a), we show the case where Rashba and Dresselhaus SOIs present simultaneously with $\Delta_R = 0.7$ and $\Delta_D = 0.3$, or vice versa. Compared to the case of individual SOIs, coupling between neighboring subbands is remarkably enhanced and more anticrossings show up. The cases where either Rashba or Dresselhaus SOI only coexists with the SOI due to the lateral confinement are shown in figures 2(c) and (d), respectively. We see that the presence of the SOI due to the lateral confinement only enhances considerably the anticrossings of spin branches in neighboring subbands and in the vicinity of $k_y = 0$. However, these anticrossings are very weak for k_ys far from zero and look like crosses in the figure. Furthermore, the two branches in each subband become approximately degenerate for larger values of k_y. The presence of the lateral SOI also reduces the energy splitting created by Rashba or Dresselhaus coupling. In addition, the energy dispersion of the nth subband in a Rashba SOI quantum wire is very similar to the energy dispersion of the $(n + 1)$th subband in a Dresselhaus SOI quantum wire for equal Δ_R and Δ_D but fixed $\Delta_T = 0.5$. We note that a similar situation has been investigated in [37], which discusses the pertinent issue more theoretically in terms of the addition of angular momentum. The lowest subband is almost degenerate and flat in the considered energy range for a quantum wire with Dresselhaus and transverse SOIs. If three types of SOI mechanisms present simultaneously (figure 2(b)), more anticrossings occur in the energy dispersion (the two cases for fixed Δ_T but reversed relative strength of Rashba and Dresselhaus SOIs are shown).

The special case, where Rashba and Dresselhaus SOIs present simultaneously and are of the same strength, should be emphasized. Figures 3(a)–(d) show the cases where non-zero spin–orbit coupling energy $\Delta_R = \Delta_D$, $\Delta_D = \Delta_T$, $\Delta_R = \Delta_T$ and $\Delta_R = \Delta_D = \Delta_T$ are all of 0.2, respectively. We see that, for $\Delta_R = \Delta_D$, the anticrossings of different subbands are almost completely canceled, and the dispersion seems to fully restore the parabolic shape with a horizontal shift for two spin branches, and thus different spin branches cross each other. This is because the quantity of $(\sigma_x \mp \sigma_y)/\sqrt{2}$ is conserved in this special case and the spin state of the electrons becomes independent of the wavevector. This conserved quantity is related to the symmetry of time reversal [15]. But for $\Delta_D =$

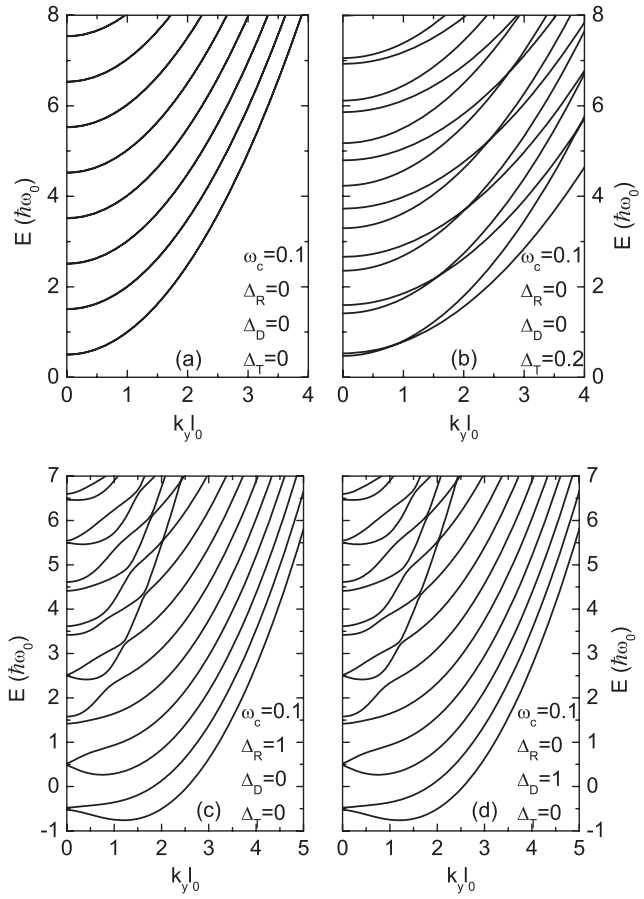

Figure 4. Energy dispersion of the spin-split subbands under a weak magnetic field of $\omega_c = 0.1\omega_0$ for cases of only one type of spin–orbit interaction present. (a) Without spin–orbit interaction. (b) $\Delta_T = 0.2$. (c) $\Delta_R = 1$. (d) $\Delta_D = 1$. (Δ_R, Δ_D and Δ_T are in units of $\hbar\omega_0$.)

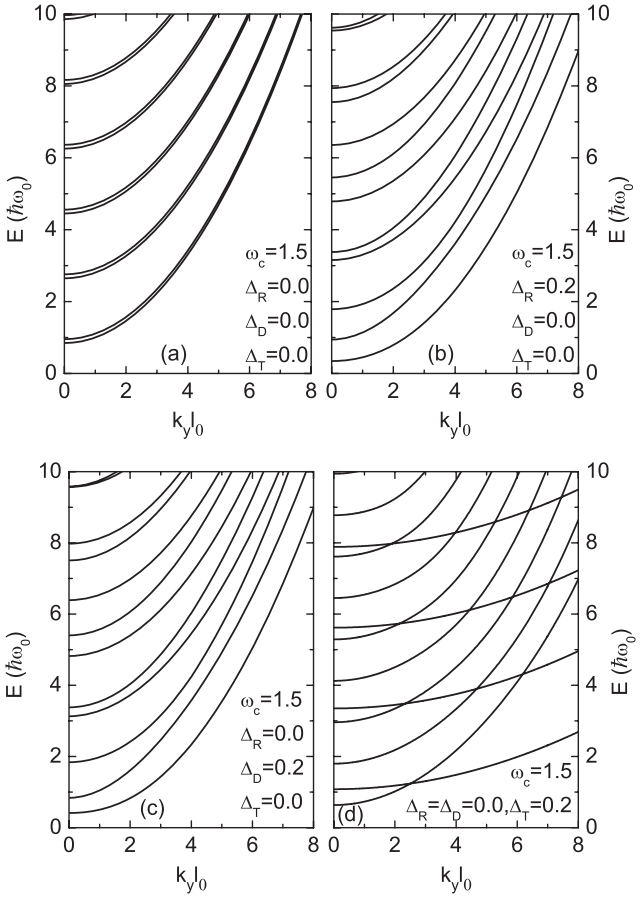

Figure 5. Energy dispersion of the spin-split subbands under a strong magnetic field of $\omega_c = 1.5\omega_0$ for cases with only one type of spin–orbit interaction present. (a) Without spin–orbit interaction. (b) $\Delta_R = 0.2$. (c) $\Delta_D = 0.2$. (d) $\Delta_T = 0.2$. (Δ_R, Δ_D and Δ_T are in units of $\hbar\omega_0$.)

Δ_T and $\Delta_R = \Delta_T$, parts of the anticrossings remain, and there is a slight difference in the energy dispersions between the cases of $\Delta_D = \Delta_T$ and $\Delta_R = \Delta_T$ (figures 3(b) and (d)). However, for $\Delta_R = \Delta_D = \Delta_T$ (figure 3(c)), all the crosses except at $k_y = 0$ become anticrosses, and there is a difference for the strength of anticrosses for different branches or at different k_y values. The special case has been emphasized by several research groups, for example, Schliemann *et al* [15] have suggested a nonballistic spin transistor based on this characteristic, though the transistor is proposed to be along the [110] crystallographic axis, whereas in the present work the quantum wires are assumed to be made along the [010] crystallographic axis.

3.2. With magnetic field

Now, we consider the influence of a perpendicular magnetic field on the subband structures, since it is important for elucidating the beating pattern in the magnetoresistance and absorption spectra of magneto-optic transitions. Figures 4(a)–(d) show the effect of a weak magnetic field of strength $\omega_c = 0.1\omega_0$ on the energy dispersion of a quantum wire. Without spin–orbit coupling (figure 4(a)), the primary effect of this weak magnetic field is to lift the degeneracy of the two different spin orientations for each subband. However, due to the weak field, the Zeeman splits are indistinguishable to the eye in figure 4(a). If the SOI due to the lateral confining potential presents (figure 4(b)), the twofold degeneracy of each subband is lifted and the separation between the two different spin orientations within each subband increases with n increasing, remarkably in contrast to the zero-field case (figures 1(b), (d) and (f)). Furthermore, the split branches have different slopes and they cross each other. With strong Rashba or Dresselhaus SOI (figures 4(c) and (d)), the dominant effect of this weak magnetic field is to lift the degeneracy of the two different spin orientations at $k_y = 0$, thus the lower spin branches of each subband develop a 'camelback' shape in the vicinity of $k_y = 0$. The anticrossing feature caused by the strong SOI at non-zero k_y is hardly affected.

Figures 5(a)–(d) show the energy dispersion of electrons in a quantum wire with (figures 5(b)–(d)) and without (figure 5(a)) an individual SOI under a strong magnetic field of $\omega_c = 1.5\omega_0$. From figure 5(a), we see that, in the absence of the SOI, the strong magnetic field lifts the twofold degeneracy of different spin orientations in each subband by the Zeeman effect. In addition, the subband separation is increased from $\hbar\omega_0$ to $\hbar\omega$, with $\omega = (\omega_c^2+\omega_0^2)^{1/2}$. Figures 5(b) and (c) show the energy dispersion with a moderate Rashba

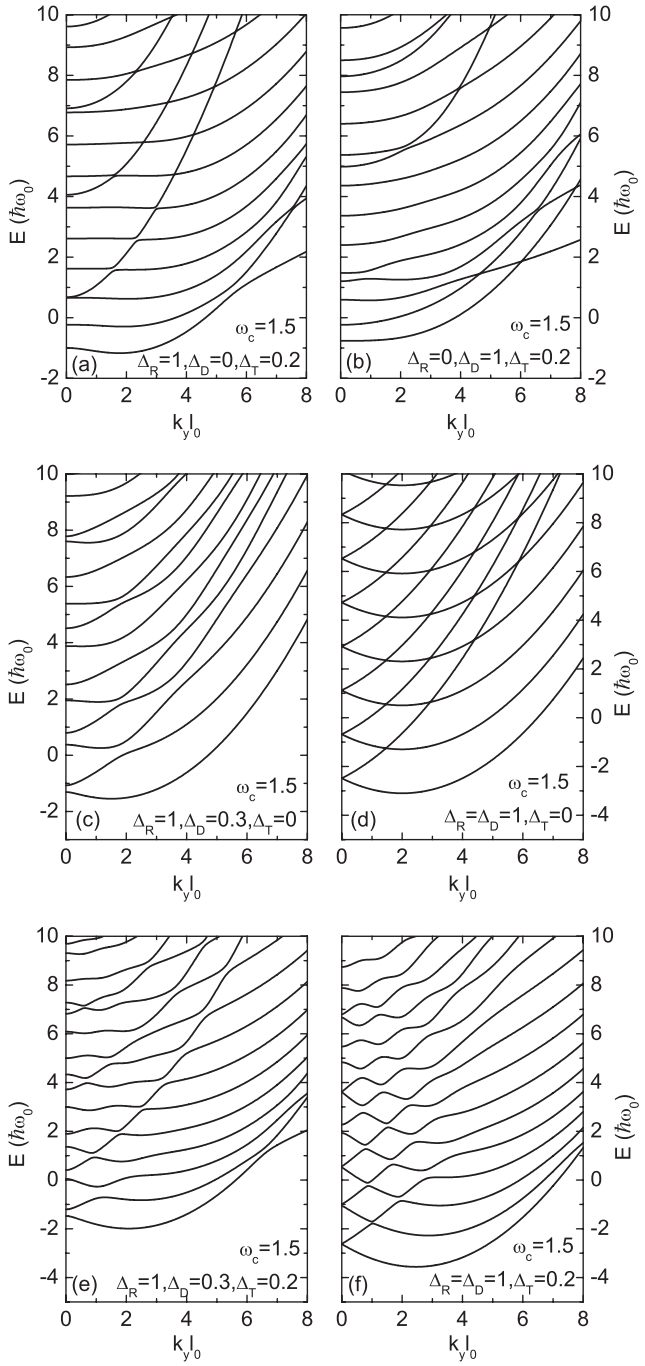

Figure 6. Energy dispersion of the spin-split subbands under a strong magnetic field of $\omega_c = 1.5\omega_0$ for cases with only at least two types of spin–orbit interactions present. (a) $\Delta_R = 1$, $\Delta_D = 0$, $\Delta_T = 0.2$. (b) $\Delta_R = 0$, $\Delta_D = 1$, $\Delta_T = 0.2$. (c) $\Delta_R = 1 \neq \Delta_D = 0.3$, $\Delta_T = 0$. (d) $\Delta_R = \Delta_D = 1$, $\Delta_T = 0$. (e) $\Delta_R = 1 \neq \Delta_D = 0.3$, $\Delta_T = 0.2$. (f) $\Delta_R = \Delta_D = 1$, $\Delta_T = 0.2$. (Δ_R, Δ_D and Δ_T are in units of $\hbar\omega_0$.)

and Dresselhaus spin–orbit coupling of $\Delta_{so}/\hbar\omega_0 = 0.2$, respectively. In contrast to the zero-field case, no remarkable anticrossing of the subbands occurs in the energy range. Also the lowest subband does not show the 'camelback' shape. Thus the magnetic field suppresses the coupling strength between different subbands. Compared to the zero magnetic field the slope of the dispersion is smaller due to the increased effective mass. Figure 5(d) shows the energy dispersion with a moderate SOI due to lateral confinement under a strong magnetic field. In this case, the branches are evidently divided into two groups with very different slopes of the energy dispersion and they cross each other.

In figure 6, we show the energy dispersion of electrons in a quantum wire under a strong magnetic field in the presence of at least two SOIs. From figures 6(a) and (b), we see that dispersions of strong Rashba and Dresselhaus SOIs coexisting with a lateral potential induced SOI are different, in contrast to the zero-field case. Figures 6(c) and (d) show the cases where Rashba and Dresselhaus SOIs are present simultaneously but with different and same strength, respectively. As in the zero-field case, anticrossings occur for different spin–orbit coupling strengths, whereas crossings occur for same spin–orbit coupling strengths. However, if the SOIs due to the three different coupling mechanisms present simultaneously (figures 6(e) and (f)), the SOI due to the transverse confinement enhances significantly anticrossings for the different coupling strength for Rashba and Dresselhaus SOIs, and converts the crossings to anticrossings for the same coupling strength for Rashba and Dresselhaus SOIs.

From the above numerical results, we see that the energy dispersion of subbands is dependent on the interplay of all different SOIs, as well as a perpendicular magnetic field. The difference in the energy dispersions may induce different transport patterns or optical transitions. For example, the number of ballistic channels (defining the conductance) is expected to be modified by changing some parameter, say, by the lateral potential Δ_T, since it modifies dramatically the subbands at the $k_y = 0$ point, even turning negative the sign of their curvatures. In addition, the degree of spin polarization should be possible to control by changing SOI strengths. All these influences on the interplay of all different SOIs on the electron transport properties are very interesting and may be demonstrated in experiments. Since we focus on the dispersion of the subbands, we will investigate these phenomena quantitatively in detail in a forthcoming paper.

4. Summary

We have made a thorough theoretical investigation of the interplay of SOIs resulting from different mechanisms, such as Rashba SOI, Dresselhaus SOI and the SOI due to the lateral parabolic confining potential, on the energy dispersion relations of the spin subbands in a quantum wire. The two cases in the absence of and in the presence of an external magnetic are investigated. We show the interplay leads to a rather complex level spectrum for different coupling parameters and for different magnetic field strengths. The difference in the energy dispersions and their induced transport or optical properties in different cases may be used to identify the existence of some type of SOI mechanism or extract the coupling parameter values. Furthermore, by changing SOI strengths via controlling the gate voltages, the number of ballistic channels, as well as the degree of spin polarization, may be expected to be modified.

Acknowledgments

This work is supported by the National Natural Science Foundation of China (under grant nos. 10834015 and 60777017), the National Basic Research Program of China (973 Program) (under grant no. 2007CB310405), the China Postdoctoral Science Foundation and the K C Wong Education Foundation, Hong Kong.

References

[1] Wolf S A, Awschalom D D, Buhrman R A, Daughton J M, von Molnár S, Roukes M L, Chtchelkanova A Y and Treger D M 2001 *Science* **294** 1488
[2] Ganichev S D, Ivchenko E L, Bel'kov V V, Tarasenko S A, Sollinger M, Weiss D, Wegscheider W and Prettl W 2002 *Nature* **417** 153
[3] Žutić I, Fabian J and Das Sarma S 2004 *Rev. Mod. Phys.* **76** 323 and references therein
[4] Yuan D W, Xu W, Zeng Z and Lu F 2005 *Phys. Rev.* B **72** 033320
[5] Wu B H and Cao J C 2006 *Phys. Rev.* B **73** 245412
Wu B H and Cao J C 2006 *Phys. Rev.* B **74** 115313
Wu B H and Cao J C 2007 *Phys. Rev.* B **75** 113303
[6] Bernardes E, Schliemann J, Lee M, Egues J C and Loss D 2007 *Phys. Rev. Lett.* **99** 076603
[7] Liu J F, Zhong Z C, Chen L, Li D, Zhang C and Ma Z 2007 *Phys. Rev.* B **76** 195304
[8] Chen L, Ma Z, Cao J C, Zhang T Y and Zhang C 2007 *Appl. Phys. Lett.* **91** 102115
[9] Li Z, Ma Z and Zhang C 2008 *Europhys. Lett.* **82** 67003
[10] Rashba E I 1960 *Sov. Phys.—Solid State* **2** 1109
Bychkov Yu A and Rashba E I 1984 *JETP Lett.* **39** 78
[11] Dresselhaus G 1955 *Phys. Rev.* **100** 580
[12] Luo J, Munekata H, Fang F F and Stiles P J 1988 *Phys. Rev.* B **38** 10142
Luo J, Munekata H, Fang F F and Stiles P J 1990 *Phys. Rev.* B **41** 7685
[13] Grundler D 2000 *Phys. Rev. Lett.* **84** 6074
[14] Datta S and Das B 1990 *Appl. Phys. Lett.* **56** 665
[15] Schliemann J, Egues J C and Loss D 2003 *Phys. Rev. Lett.* **90** 146801
[16] Rashba E I and Efros Al L 2003 *Phys. Rev. Lett.* **91** 126405
[17] Kiselev A A and Kim K W 2001 *Appl. Phys. Lett.* **78** 775
[18] Governale M, Boese D, Zülicke U and Schroll C 2002 *Phys. Rev.* B **65** 140403
[19] Governale M and Zülicke U 2002 *Phys. Rev.* B **66** 073311
[20] Zülicke U and Governale M 2002 *Phys. Rev.* B **65** 205304
[21] Eto M, Hayashi T and Kurotani Y 2005 *J. Phys. Soc. Japan* **74** 1934
[22] Zhai F and Xu H Q 2007 *Phys. Rev.* B **76** 035306
[23] Zhai F, Chang K and Xu H Q 2008 *Appl. Phys. Lett.* **92** 102111
[24] Moroz A V and Barnes C H W 1999 *Phys. Rev.* B **60** 14272
[25] Perroni C A, Bercioux D, Ramaglia V M and Cataudella V 2007 *J. Phys.: Condens. Matter* **19** 186227
[26] Mireles F and Kirczenow G 2001 *Phys. Rev.* B **64** 024426
[27] Moroz A V and Barnes C H W 2000 *Phys. Rev.* B **61** R2464
[28] Knobbe J and Schäpers Th 2005 *Phys. Rev.* B **71** 035311
[29] Li Y X, Guo Y and Li B Z 2005 *Phys. Rev.* B **72** 075321
[30] Debald S and Kramer B 2005 *Phys. Rev.* B **71** 115322
[31] Sato Y, Gozu S, Kikutani T and Yamada S 1999 *Physica* E **272** 114
[32] Schäpers Th, Knobbe J and Guzenko V A 2004 *Phys. Rev.* B **69** 235323
[33] Guzenko V A, Knobbe J, Hardtdegen H, Schäpers Th and Bringer A 2006 *Appl. Phys. Lett.* **88** 032102
[34] Lehnen P, Schäpers Th, Kaluza N, Thillosen N and Hardtdegen H 2007 *Phys. Rev.* B **76** 205307
[35] Bandyopadhyay S and Sarkar S 2006 *Appl. Phys. Lett.* **88** 183108
[36] Upadhyaya P, Pramanik S and Bandyopadhyay S 2008 *Phys. Rev.* B **77** 155439
[37] Das B, Datta S and Reifenberger R 1990 *Phys. Rev.* B **41** 8278
[38] Malet F, Lipparini E, Barranco M and Pi M 2006 *Phys. Rev.* B **73** 125302
[39] Lipparini E, Barranco M, Malet F, Pi M and Serra L 2006 *Phys. Rev.* B **74** 115303
[40] Valín-Rodríguez M and Nazmitdinov R G 2006 *Phys. Rev.* B **73** 235306
[41] Pramanik S, Bandyopadhyay S and Cahay M 2007 *Phys. Rev.* B **76** 155325
[42] Lee H C and Eric Yang S-R 2005 *Phys. Rev.* B **72** 245338
[43] Cahay M and Bandyopadhyay S 2004 *Phys. Rev.* B **69** 045303
[44] Pershin Yu V, Nesteroff J A and Privman V 2004 *Phys. Rev.* B **69** 121306(R)
[45] Bandyopadhyay S, Pramanik S and Cahay M 2004 *Superlatt. Microstruct.* **35** 67
[46] Tserkovnyak Y and Halperin B I 2006 *Phys. Rev.* B **74** 245327
[47] Sánchez D, Serra L and Choi M-S 2008 *Phys. Rev.* B **77** 035315
[48] Greiner W 1998 *Quantum Mechanics: Special Chapters* (Berlin: Springer)
[49] Bandyopadhyay S and Cahay M 2004 *Appl. Phys. Lett.* **85** 1814
[50] Häusler W 2001 *Phys. Rev.* B **63** 121310(R)